

Efficient Irregular Wavefront Propagation Algorithms on Hybrid CPU-GPU Machines

George Teodoro*, Tony Pan, Tahsin Kurc, Jun Kong, Lee Cooper, Joel Saltz

*Center for Comprehensive Informatics and Biomedical Informatics Department,
Emory University, Atlanta, GA 30322*

Abstract

In this paper, we address the problem of efficient execution of a computation pattern, referred to here as the irregular wavefront propagation pattern (IWPP), on hybrid systems with multiple CPUs and GPUs. The IWPP is common in several image processing operations. In the IWPP, data elements in the wavefront propagate waves to their neighboring elements on a grid if a propagation condition is satisfied. Elements receiving the propagated waves become part of the wavefront. This pattern results in irregular data accesses and computations. We develop and evaluate strategies for efficient computation and propagation of wavefronts using a multi-level queue structure. This queue structure improves the utilization of fast memories in a GPU and reduces synchronization overheads. We also develop a tile-based parallelization strategy to support execution on multiple CPUs and GPUs. We evaluate our approaches on a state-of-the-art GPU accelerated machine (equipped with 3 GPUs and 2 multicore CPUs) using the IWPP implementations of two widely used image processing operations: morphological reconstruction and euclidean distance transform. Our results show significant performance improvements on GPUs. The use of multiple CPUs and GPUs cooperatively attains speedups of $50\times$ and $85\times$ with respect to single core CPU executions for morphological reconstruction and euclidean distance transform, respectively.

Keywords: Irregular Wavefront Propagation Pattern, GPGPU, Cooperative CPU-GPU Execution, Heterogeneous Environments, Morphological Reconstruction, Euclidean Distance Transform

*Corresponding author

Email addresses: george.teodoro@emory.edu (George Teodoro), tony.pan@emory.edu (Tony Pan), tkurc@emory.edu (Tahsin Kurc), jun.kong@emory.edu (Jun Kong), lee.cooper@emory.edu (Lee Cooper), jhsaltz@emory.edu (Joel Saltz)

1. Introduction

This paper investigates efficient parallelization on hybrid CPU-GPU systems of operations or applications whose computation structure includes what we call the *irregular wavefront propagation pattern* (IWPP) (see Algorithm 1). Our work is motivated by the requirements of analysis of whole slide tissue images in biomedical research. With rapid improvements in sensor technologies and scanner instruments, it is becoming feasible for research projects and healthcare organizations to gather large volumes of microscopy images. We are interested in enabling more effective use of large datasets of high resolution tissue slide images in research and patient care. A typical image from state-of-the-art scanners is about $50K \times 50K$ to $100K \times 100K$ pixels in resolution. A whole slide tissue image is analyzed through a cascade of image normalization, object segmentation, object feature computation, and object/image classification stages. The segmentation stage is expensive and composed of a pipeline of substages. The most expensive substages are built on several low-level operations, notably morphological reconstruction [55] and distance transform [53]. Efficient implementation of these operations is necessary to reduce the cost of image analysis.

Processing a high resolution image on a single CPU system can take hours. The processing power and memory capacity of graphics processing units (GPUs) have rapidly and significantly improved in recent years. Contemporary GPUs provide extremely fast memories and massive multi-processing capabilities, exceeding those of multi-core CPUs. The application and performance benefits of GPUs for general purpose processing have been demonstrated for a wide range of applications [14, 41, 49, 43, 6, 34]. As a result, CPU-GPU equipped machines are emerging as viable high performance computing platforms for scientific computation [52].

The processing structures of the morphological reconstruction and distance transform operations bear similarities and include the IWPP on a grid. The IWPP is characterized by one or more source grid points from which waves originate and the irregular shape and expansion of the wave fronts. The composition of the waves is dynamic, data dependent, and computed during execution as the waves are expanded. Elements in the front of the waves work as the sources of wave propagations to neighbor elements. A propagation occurs only when a given *propagation condition*, determined based on the value of a wavefront element and the values of its neighbors, is satisfied. In practice, each element in the propagation front represents an independent wave propagation; interaction between waves may even change the direction of the propagation. In the IWPP only those elements in the wavefront are the ones effectively contributing for the output results. Because of this property, an efficient implementation of irregular wavefront propagation can be accomplished using an auxiliary container structure, e.g., a queue, set, or stack, to keep track of active elements forming the wavefront. The basic components of the IWPP are shown in Algorithm 1.

In this algorithm, a set of elements in a multi-dimensional grid space (D) are selected to form the initial wavefront (S). These active elements then act as wave

Algorithm 1 Irregular Wavefront Propagation Pattern (IWPP)

```
1:  $D \leftarrow$  data elements in a multi-dimensional space
2: {Initialization Phase}
3:  $S \leftarrow$  subset active elements from  $D$ 
4: {Wavefront Propagation Phase}
5: while  $S \neq \emptyset$  do
6:   Extract  $e_i$  from  $S$ 
7:    $Q \leftarrow N_G(e_i)$ 
8:   while  $Q \neq \emptyset$  do
9:     Extract  $e_j$  from  $Q$ 
10:    if  $PropagationCondition(D(e_i), D(e_j)) = \text{true}$  then
11:       $D(e_j) \leftarrow Update(D(e_i))$ 
12:      Insert  $e_j$  into  $S$ 
```

propagation sources in the wavefront propagation phase. During propagation phase, a single element (e_i) is extracted from the wavefront and its neighbors ($Q \leftarrow N_G(e_i)$) are identified. The neighborhood of an element e_i is defined by a discrete grid G , also referred to as the structuring element. The element e_i tries to propagate the wavefront to each neighbor $e_j \in Q$. If the propagation condition ($PropagationCondition$), based on the values of e_i and e_j , is satisfied, the value of the element e_j ($D(e_j)$) is updated, and e_j is inserted in the container (S). The assignment operation performed in Line 11, as a consequence of the wave expansion, is expected to be commutative and atomic. That is, the order in which elements in the wavefront are computed should not impact the algorithm results. The wavefront propagation process continues until stability is reached; i.e., until the wavefront container is empty.

The IWPP is not unique to morphological reconstruction and distance transform. Core computations in several other image processing methods contain a similar structure: Watershed [56], Euclidean skeletons [28], and skeletons by influence zones [23]. Additionally, Delaunay triangulations [33], Gabriel graphs [15] and relative neighborhood graphs [51] can be derived from these methods. Another example of the IWPP is the shortest-path computations on a grid which contains obstacles between source points and destination points (e.g., shortest path calculations in integrated circuit designs). A high performance implementation of the IWPP can benefit these methods and applications.

The traditional wavefront computation is common in many scientific applications [57, 3, 2]. It is also a well-known parallelization pattern in high performance computing. In the classic wavefront pattern, data elements are laid out in a multi-dimensional grid. The computation of an element on the wavefront depends on the computation of a set of neighbor points. The classic wavefront pattern has a regular data access and computation structure in that the wavefront starts from a corner point of the grid and sweeps the grid diagonally from one region to another. The morphological reconstruction and distance transform operations could potentially be implemented in the form of

iterative traditional wavefront computations. However, the IWPP offers a more efficient execution structure, since it avoids touching and computing on data points that do not contribute to the output. The IWPP implementation on a hybrid machine consisting of multiple CPUs and GPUs is a challenging problem. The difficulties with IWPP parallelization are accentuated by the irregularity of the computation that is spread across the input domain and evolves during the computation as active elements change.

In this paper, we propose, implement, and evaluate parallelization strategies for efficient execution of IWPP computations on large grids (e.g., high resolution images) on a machine with multiple CPUs and GPUs. The proposed strategies can take full advantage this computation pattern characteristics to achieve efficient execution on multicore CPU and GPU systems. The contributions of our work can be summarized as follows:

- We identify a computation pattern commonly found in several analysis operations: the irregular wavefront propagation pattern.
- We develop an efficient GPU implementation of the IWPP algorithm using a multi-level queue structure. The multi-level queue structure improves the utilization of fast memories in a GPU and reduces synchronization overheads among GPU threads. To the best of our knowledge this is the first work to implement this pattern for GPU accelerated environments.
- We develop efficient implementations of the morphological reconstruction and distance transform operations on a GPU using the GPU-enabled IWPP algorithm. These are the first GPU-enabled IWPP-based implementations of morphological reconstruction and distance transform. The morphological reconstruction implementation achieves much better performance than a previous implementation based on raster/anti-raster scans of the image. The output results for morphological reconstruction and distance transform are exact regarding their sequential counterparts.
- We extend the GPU implementation of the IWPP to support processing of images that do not fit in GPU memory through coordinated use of multiple CPU cores and multiple GPUs on the machine.

We perform a performance evaluation of the IWPP implementations using the morphological reconstruction and distance transform operations on a state-of-the-art hybrid machine with 12 CPU cores and 3 NVIDIA Tesla GPUs. Significant performance improvements were observed in our experiments. Speedups of $50\times$ and $85\times$ were achieved, as compared to the single CPU core execution, respectively, for morphological reconstruction and euclidean distance transform when all the CPU cores and GPUs were used in a coordinated manner. We were able to compute morphological reconstruction on a $96K \times 96K$ -pixel image in 21 seconds and distance transform on a $64K \times 64K$ -pixel image in 4.1 seconds. These performances make it feasible to analyze very high resolution images rapidly and conduct large scale studies.

The manuscript is organized as follows. Section 2 presents the use of the IWPP on image analysis, including preliminary definitions and the implementation of use case algorithms: morphological reconstruction and euclidean distance transform. The IWPP parallelization strategy and its support in GPUs are discussed in Section 3. The extensions for multiple GPUs and cooperative CPU-GPU execution are described in Section 4. The experimental evaluation is presented in Section 5. Finally, Sections 6 and 7, respectively, present the related work and conclude the paper.

2. Irregular Wavefront Propagation Pattern in Image Analysis

We describe two morphological algorithms, *Morphological Reconstruction* and *Euclidean Distance Transform*, from the image analysis domain to illustrate the IWPP. Morphological operators are basic operations used by a broad set of image processing algorithms. These operators are applied to individual pixels and are computed based on the current value of a pixel and pixels in its neighborhood. A pixel p is a neighbor of pixel q if $(p, q) \in G$. G is usually a 4-connected or 8-connected square grid. $N_G(p)$ refers to the set of pixels that are neighbors of $p \in \mathbb{Z}^n$ according to G ($N_G(p) = \{q \in \mathbb{Z}^n | (p, q) \in G\}$). Input and output images are defined in a rectangular domain $D_I \in \mathbb{Z}^n \rightarrow \mathbb{Z}$. The value $I(p)$ of each image pixel p assumes 0 or 1 for binary images. For gray scale images, the value of a pixel comes from a set $\{0, \dots, L - 1\}$ of gray levels from a discrete or continuous domain.

2.1. Morphological Reconstruction Algorithms

Morphological reconstruction is one of the elementary operations in image segmentation [55]. When applied to binary images, it pulls out the connected components of an image identified by a *marker* image. Figure 1 illustrates the process. The dark patches inside three objects in image I (also called the mask image) on the left correspond to the marker image J . The result of the morphological reconstruction is shown on the right.

Quando aplicado em imagens binárias, gera os componentes conectados identificados por uma marker image

marker image J

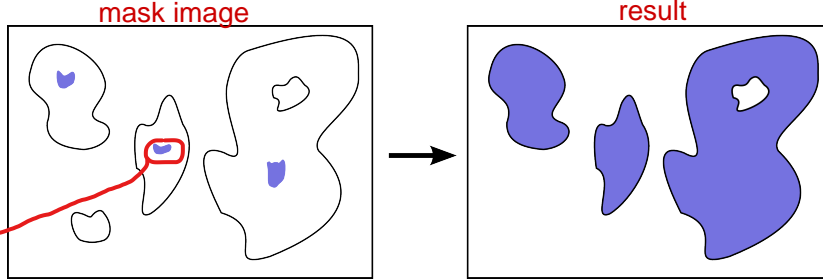


Figure 1: Binary morphological reconstruction from markers. The markers are the dark patches inside three of the objects in the image on the left. The image on the right shows the reconstructed objects and the final binary image after the application of morphological reconstruction.

a reconstrução é feita apenas dos componentes marcados?

Sim

Morphological reconstruction can also be applied to gray scale images. Figure 2 illustrates the process of gray scale morphological reconstruction in 1-dimension. The marker intensity profile is propagated spatially but is bounded by the mask image's intensity profile. The primary difference between binary and gray scale morphological reconstruction algorithms is that in binary reconstruction, any pixel value change is necessarily the final value change, whereas a value update in gray scale reconstruction may later be replaced by another value update. In color images, morphological reconstruction can be applied either to individual channels (e.g., the Red, Green, and Blue channels in an RGB image) or to gray scale values computed by combining the channels.

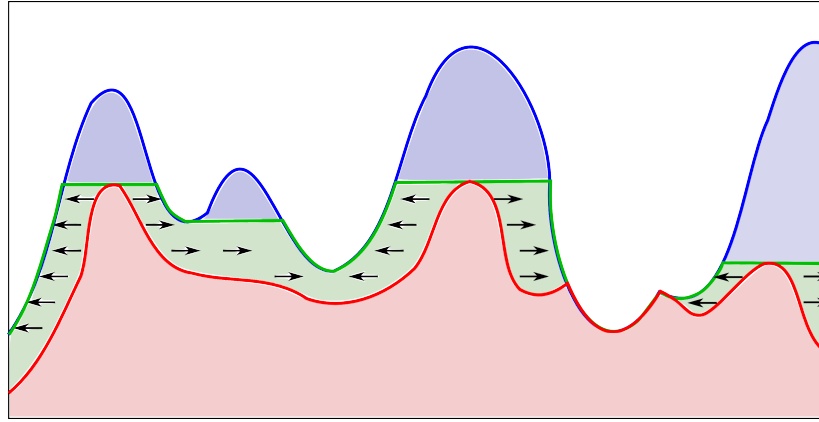


Figure 2: Gray scale morphological reconstruction in 1-dimension. The marker image intensity profile is represented as the red line, and the mask image intensity profile is represented as the blue line. The final image intensity profile is represented as the green line. The arrows show the direction of propagation from the marker intensity profile to the mask intensity profile. The green region shows the changes introduced by the morphological reconstruction process.

The morphological reconstruction $\rho_I(J)$ of mask I from marker image J is done by performing elementary dilations (i.e., dilations of size 1) in J by G , the structuring element. An elementary dilation from a pixel p corresponds to propagation from p to its immediate neighbors in G . The basic algorithm carries out elementary dilations successively over the entire image J , updates each pixel in J with the pixelwise minimum of the dilation's result and the corresponding pixel in I (i.e., $J(p) \leftarrow (\max\{J(q), q \in N_G(p) \cup \{p\}\}) \wedge I(p)$, where \wedge is the pixelwise minimum operator), and stops when *stability* is reached, i.e., when no more pixel values are modified. Several morphological reconstruction algorithms for gray scale images have been developed by Vincent [55] based on this core technique. We present brief descriptions of these algorithms below and refer the reader to the original paper for more details.

$J(p)$ é o mínimo entre o valor de p na máscara e o máximo valor entre p e seus vizinhos



É o mínimo entre os dois valores?

isso é feito para limitar ao valor da máscara?

Sequential Reconstruction (SR): Pixel value propagation in the marker image is computed by alternating raster and anti-raster scans. A raster scan starts from the pixel at $(0, 0)$ and proceeds to the pixel at $(N - 1, M - 1)$ in a row-wise

manner, while an anti-raster starts from the pixel at $(N - 1, M - 1)$ and moves to the pixel at $(0, 0)$ in a row-wise manner. Here, N and M are the resolution of the image in x and y dimensions, respectively. In each scan, values from pixels in the upper left or the lower right half neighborhood are propagated to the current pixel in raster or anti-raster fashion, respectively. The raster and anti-raster scans allow for changes in a pixel to be propagated in the current iteration. The SR method iterates until stability is reached, i.e., no more changes in pixels are computed.

Queue-based Reconstruction (QB): In this method, a first-in first-out (FIFO) queue is initialized with pixels in the regional maxima. The computation then proceeds by removing a pixel from the queue, scanning the pixel's neighborhood, and queuing the neighbor pixels whose values have been changed. The overall process continues until the queue is empty.

Fast Hybrid Reconstruction (FH): The computation of the regional maxima needed to initialize the queue in QB incurs significant computational cost. The FH approach incorporates the characteristics of the SR and QB algorithms to reduce the cost of initialization, and is about one order of magnitude faster than the others. It first makes one pass using the raster and anti-raster orders as in SR. After that pass, it continues the computation using a FIFO queue as in QB. A pseudo-code implementation of FH is presented in Algorithm 2, N_G^+ and N_G^- denote the set of neighbors in $N_G(p)$ that are reached before and after touching pixel p during a raster scan.

2.2. Euclidean Distance Transform

The distances transform (DT) operation computes a distance map M from a binary input image I , where for each pixel $p \in I$ the pixel's value in M , $M(p)$, is the smallest distance from p to a background pixel. DT is a fundamental operator in shape analysis, which can be used for separation of overlapping objects in watershed based segmentation [56, 39]. It can also be used in the calculation of morphological operations [8] as erosion and dilation and the computation of Voronoi diagrams and Delaunay triangulation [53].

The definition of DT is simple, but historically it has been hard to achieve good precision and efficiency for this operation. For a comprehensive discussion of algorithms for calculation of distance transform, we refer the reader to the survey by Fabbri et al. [12]. The first DT algorithms were proposed by Rosenfeld and Pfaltz [38]. These algorithms were based on raster/anti-raster scans strategies to calculate non-Euclidean metrics such as cityblock and chessboard, which at that time were used as approximations to the Euclidean distance. Danielsson proposed an algorithm [11] to compute Euclidean DT that propagates information of the nearest background pixel using neighborhood operators in a raster/anti-raster scan manner. With this strategy, a two-element vector with location information of the nearest background pixel is propagated through neighbor pixels. Intrinsically, it builds Voronoi diagrams where regions are formed by pixels with the same nearest background pixel.

Algorithm 2 Fast Hybrid Gray scale Morphological Reconstruction Algorithm

Input*I: mask image**J: marker image.*

```
1: {Initialization Phase}
2: Scan  $I$  and  $J$  in raster order.
3: Let  $p$  be the current pixel
4:  $J(p) \leftarrow (\max\{J(q), q \in N_G^+(p) \cup \{p\}\}) \wedge I(p)$ 
5: Scan  $I$  and  $J$  in anti-raster order.
6: Let  $p$  be the current pixel
7:  $J(p) \leftarrow (\max\{J(q), q \in N_G^-(p) \cup \{p\}\}) \wedge I(p)$ 
8: if  $\exists q \in N_G^-(p) \mid J(q) < J(p)$  and  $J(q) < I(q)$ 
9:   queue.add(p)
10: {Wavefront Propagation Phase}
11: while queue.empty() = false do
12:    $p \leftarrow \text{dequeue}()$ 
13:   for all  $q \in N_G(p)$  do
14:     if  $J(q) < J(p)$  and  $I(q) \neq J(q)$  then
15:        $J(q) \leftarrow \min\{J(p), I(q)\}$ 
16:       queue.add(q)
```

Danielsson's algorithm is not an exact algorithm. The Voronoi diagram is not connected in a discrete space, though it is in the continuous space. Hence, the Voronoi diagram computation through a neighborhood based operator introduces approximation errors as illustrated in Figure 3. Nevertheless, approximation errors introduced by the algorithm are small and bound by a mathematical framework. Approximations computed by this algorithm have been found to be sufficient in practice for several applications [9, 13, 50]. Moreover, some of the exact euclidean distance transform algorithms [8, 42, 30] are implemented as a post-processing phase to Danielsson's algorithm, in which approximation errors are resolved.

Algorithm 3 presents an irregular wavefront propagation based approach to efficiently compute the single neighborhood approximation of DT. In the *initialization phase* a pass on the input is performed to identify and queue pixels forming the initial wavefront. In Lines 2 and 3, Voronoi diagram (VR) that holds the current nearest background pixel for each image pixel is initialized. Each background pixel will itself be its nearest pixel, while the foreground pixels will initially point to a pixel virtually at infinite distance (*inf*). The *inf* pixel is such that for each pixel p , p is closer to any other pixel in the image domain than it is to the *inf* pixel. At the end of the initialization phase, background pixels with a foreground neighbor (contour pixels) are added to a queue for propagation (Lines 4 and 5).

The *wavefront propagation phase* of the EDT is carried out in Lines 7 to 12. During each iteration, a pixel p is removed from the queue. The pixel's

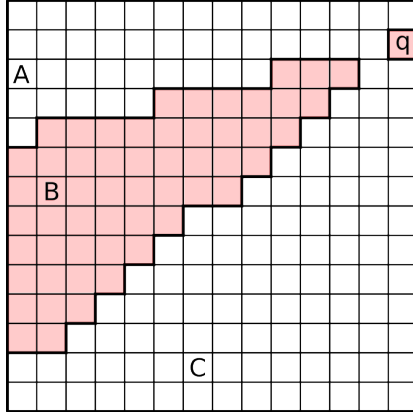


Figure 3: Errors introduced by neighborhood propagation in the euclidean distance transform operation using an 8-connected neighborhood method (Cuisenaire and Macq [8]). Pixel q is closer to object B than it is to A and C. However, q is not neighbor to any pixel in the connected Voronoi diagram starting at B. The distance value assigned to q , $M(q)$, would be $\sqrt{170}$ (about 13.038), instead of $\sqrt{169}$ (13) in the exact case.

nearest background pixel is propagated to the neighbors through a neighborhood operator. For each neighbor pixel q , if the distance of q to the current assigned nearest background pixel ($\text{DIST}(q, VR(q))$) is greater than the distance of q to the nearest background pixel of p ($\text{DIST}(q, VR(p))$), the propagation occurs. In that case, the nearest background pixel of q is updated with that of p (Line 11), and q is added to the queue for propagation. After the propagation phase is completed, the distance map is computed from the Voronoi diagram.

As presented in [8], using a sufficiently large neighborhood (structuring element) will guarantee the exactness of this algorithm. In addition, the wavefront propagation method could be extended as shown in [53] to compute the exact distance transform. To include these extensions, however, another queue would have to be used, increasing the algorithm cost. As discussed before, Danielsson’s distance transform provides acceptable results for a large number of applications [9, 13]. We have employed this version in our image analysis applications.

3. Implementation of Irregular Wavefront Propagation Pattern on a GPU

We first describe the strategy for parallel execution of the IWPP on GPUs. We then present a parallel queue data structure that is fundamental to efficiently tracking data elements in the wavefront. In the last two sections, we describe the GPU-enabled implementations of the two operations presented in Section 2.

3.1. Parallelization Strategy

After the initialization phase of the IWPP, active data elements forming the initial wavefront are put into a global queue for computation. To allow parallel

Algorithm 3 Wavefront Propagation-based Distance Transform Algorithm

Input: I : mask image

Output: M : distance map image

FG: Foreground; **BG:** Background De onde vem essas duas matrizes? Como Elas são feitas?
usando FH?

```
1: {Initialization Phase}
2: for all  $p \in D_I$  do          o que é  $D_I$ ? todos os pixels da imagem
3:    $VR(p) = (p == BG) ? p : inf$ 
4:   if  $I(p) == BG$  and  $\exists q \in N_G(p) | I(q) == FG$  then
5:     queue.add(p)
6: {Wavefront Propagation Phase}
7: while queue.empty() = false do
8:    $p \leftarrow$  dequeue()
9:   for all  $q \in N_G(p)$  do
10:    if  $DIST(q, VR(p)) < DIST(q, VR(q))$  then
11:       $VR(q) = VR(p)$ 
12:      queue.add(q)
13: for all  $p \in D_I$  do
14:    $M(p) = DIST(p, VR(p))$ 
```

execution, the data elements in the global queue are partitioned into a number of smaller queues. Each of these queues is assigned to a GPU thread block. Each block can carry out computations independent of the other blocks. This partitioning and mapping strategy reduces the communication and synchronization costs to access the global queue. With this strategy, it is not necessary to employ expensive inter-block synchronizations [58] or continuously utilize system level *Memory Fence Operations* to assert queue consistency across GPU multi-processors.

The execution of each neighborhood operator is performed considering the value of the current data element being processed (p) and that of each data element in the neighborhood ($q \in N_G(p)$). To correctly perform this computation in parallel, it is necessary to guarantee atomicity in updates on neighbor data elements (q). This can only be achieved at the cost of extra synchronization overheads. Fortunately, the use of atomic compare-and-swap (CAS) operations is sufficient to solve this race condition. The efficiency of atomic operations in GPUs have been significantly improved in the last generation of NVIDIA GPUs (Fermi) [31] because of the use of cache memory. Atomic operations obviously still are more efficient in cases where threads do not concurrently try to update the same memory address. When multiple threads attempt to update the same memory location, they are serialized in order to ensure correct execution. As a result, the number of operations successfully performed per cycle might be drastically reduced [31]. To lessen the impact of potential serialization, our GPU parallelization employs data element level parallelism which allows for data elements queued for computation to be independently processed.

seleção de pontos ideal para diminuir concorrência?

Algorithm 4 Wavefront propagation phase on a GPU

```

1: {Split initial queue equally among thread blocks}
2: while queue_empty() = false do
3:   while ( $p = \text{dequeue}(\dots)$ )! = EMPTY do in parallel
4:     for all  $q \in N_G(p)$  do
5:       repeat
6:          $\text{curValueQ} = I(q)$ 
7:         if  $\text{PropagationCondition}(I(p), \text{curValueQ})$  then isso garante que não houve alteração no valor?
8:            $\text{oldval} = \text{atomicCAS}(\&I(q), \text{op}(I(p)), \text{curValueQ})$ 
9:           if  $\text{oldval} \neq \text{curValueQ}$  then
10:             queue.add(q)
11:             break;
12:           else
13:             break;
14:       until True → ? ?
15:     queue_swap_in_out()

```

The GPU-based implementation of the propagation operation is presented in Algorithm 4. After splitting the initial queue, each block of threads enter into a loop in which data elements are dequeued in parallel and processed, and new data elements may be added to the local queue as needed. This process continues until the queue is empty. Within each loop, the data elements queued in the last iteration are uniformly divided among the threads in the block and processed in parallel (Lines 3–14 in Algorithm 4). The value of each queued data element p is compared to every data element q in its neighborhood. An atomic operation is performed when a neighbor data element q should be updated ($\text{PropagationCondition}$ is evaluated true). The value of data element q before the compare and swap operation is returned (oldval) and used to determine whether its value has really been changed (Line 9 in Algorithm 4). This step is necessary because there is a chance that another thread might have changed the value of q between the time the data element's value is read to perform the propagation condition test and the time the atomic operation is performed (Lines 6–8 in Algorithm 4). If the atomic compare and swap operation performed by the current thread has changed the value of data element q , q is added to the queue for processing in the next iteration of the loop. Even with this control, it is possible that between the test in line 9 and the addition to the queue, the data element q may have been modified again. In this case, q is added multiple times to the queue. Although it impacts the performance, the correctness of the algorithm is not affected because the update operations replace the value of q via a commutative and atomic assignment operation.

After computing the data elements from the last iteration, data elements that are added to the queue in the current iteration are made available for the next iteration. Elements used as input in one iteration and those queued during the propagation are stored in different queues. The process of mak-

ing elements queued available includes swapping the input and output queues (`queue_swap_in_out()`; Lines 15). As described in the next section, the choice to process data elements in rounds, instead of making each data element inserted into the queue immediately accessible, is made in our design to implement a queue with very efficient read performance (dequeue performance) and with low synchronization costs to provide consistency among threads when multiple threads read from and write to the queue. When maximum and minimum operations are used in the propagation condition test, `atomicCAS` may be replaced with an `atomicMax` or `atomicMin` operation to improve performance.

Since elements in the queue are divided among threads for parallel computation, the order in which the elements will be processed cannot be pre-determined. It is thus necessary for the correctness of the parallel execution that the update and assignment operations in the wave propagation phase are commutative and atomic. In practice, the order is not important for most analysis methods based on the IWPP, including the example operations presented in this paper.

3.2. Parallel Queue Implementation and Management

A parallel queue is used to keep track of elements in the wavefront. An efficient parallel queue for GPUs is a challenging problem [17, 20, 27]. A straight forward implementation of a queue, as presented by Hong et al. [17], could be done by employing an array to store items in sequence and using atomic additions to calculate the position where the item should be inserted, as presented in the code bellow.

```
AddQueue(int* q_idx, type_t* q, type_t item) {
    int old_idx = AtomicAdd(q_idx, 1);
    q[old_idx] = item;
}
```

Hong et al. stated that this solution worked well for their use case. The use of atomic operations, however, is very inefficient when the queue is heavily employed as in our case. Moreover, a single queue that is shared among all thread blocks introduces additional overheads to guarantee data consistency across the entire device. It may also require inter-block synchronization primitives [58] to synchronize threads from multiple block that are not standard methods supported by CUDA.

To avoid these inefficiencies, we have designed a parallel queue that operates independently in a per thread block basis to avoid inter-block communication. In order to exploit the fast memories in a GPU for fast write and read accesses, the queue is implemented as multiple levels of queues (as depicted in Figure 4): (i) Per-Thread queues (TQ) which are very small queues private to each thread, residing in the shared memory; (ii) Block Level Queue (BQ) which is also in the shared memory, but is larger than TQ. Write operations to the block level queue are performed in thread warp-basis; and (iii) Global Block Level Queue (GBQ) which is the largest queue and uses the global memory of the GPU to accumulate data stored in BQ when the size of BQ exceeds the shared memory size.

o que é warp-basis?
grupos de threads?

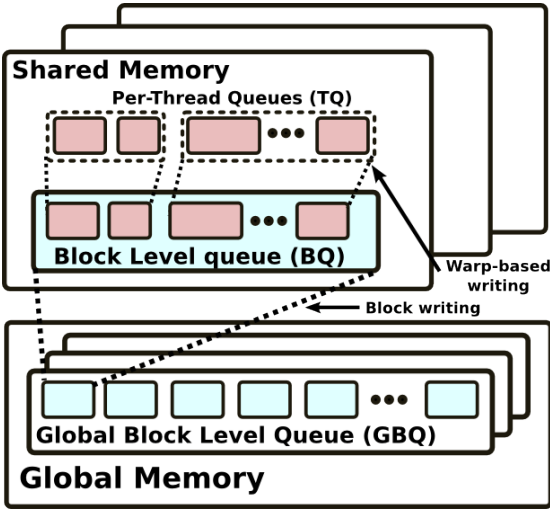


Figure 4: Multi-level parallel queue.

In our queue implementation, each thread maintains an independent queue (TQ) that does not require any synchronization to be performed. In this way threads can efficiently store data elements from a given neighborhood in the queue for computation. Whenever this level of queue is full, it is necessary to perform a warp level communication to aggregate items stored in the local queues and write them to BQ. In this phase, a parallel thread warp prefix-sum is performed to compute the total number of items queued in individual TQs. A single shared memory atomic operation is performed at the Block Level Queue to identify the position where the warp of threads should write their data. This position is returned, and the warp of threads write their local queues to BQ.

Whenever a BQ is full, the threads in the corresponding thread block are synchronized. The current size of the queue is used in a single operation to calculate the offset in GBQ from which the BQ should be stored. After this step, all the threads in the thread block work collaboratively to copy in parallel the contents of QB to GBQ. This data transfer operation is able to achieve high throughput, because the memory accesses are coalesced. It should be noted that, in all levels of the parallel queue, an array is used to hold the queue content. While the contents of TQ and BQ are copied to the lower level queues when full, GBQ does not have a lower level queue to which its content can be copied. In the current implementation, the size of GBQ is initialized with a fixed tunable memory space. If the limit of GBQ is reached during an iteration of the algorithm, excess data elements are dropped and not stored. The GPU method returns a boolean value to CPU to indicate that some data elements have been dropped during the execution of the method kernel. In that case, the wavefront propagation algorithm has to be re-executed, but using the output of the previous execution as input, because this output already holds a partial solution of the problem. Recomputing using the output of the previous step as

input will result in the same solution as if the execution was carried out in a single step.

While adding new items to the queue requires a number of operations to guarantee consistency, the read operations can be performed without introducing synchronization. This is possible by partitioning input data elements statically among threads, which keep consuming the data elements until all items are computed. The drawbacks of a static partition of the queue and work within a loop iteration are minimum, because the computation costs of the queued data elements are similar; only a minor load imbalance is introduced with this solution. Moreover, the queued data elements are repartitioned at each new iteration of the loop. A high level description of the *dequeue* function is presented below. In this function, the value of the item is initialized to a default code corresponding to an empty queue. Then, the queue index corresponding to the next item to be returned for that particular thread is calculated, based on the size of the thread block (*block_size*), the number of iterations already computed by this thread warp (*iter*), and the identifier of that thread in the block.

```
type_t DeQueue(int q_size, type_t* q, int iter) {
    type_t item = QUEUE_EMPTY;
    queue_idx = tid_in_block + iter * block_size;
    if(queue_idx < q_size){
        type_t item = q[queue_idx];
    }
    return item; }
```

3.3. GPU-enabled Fast Hybrid Morphological Reconstruction

In this section, we present how the GPU-based version of the Fast Hybrid Reconstruction algorithm, referred to in this paper as FH-GPU, is implemented (see Algorithm 5).

The first stage of FH, as is described in Section 2.1, consists of the raster and anti-raster scans of the image. This stage has a regular computation pattern that operates on all pixels of the image. An efficient GPU implementation of the SR algorithm, including the raster and anti-raster scan stage, has been done by Pavel Karas [20]. This implementation is referred to as SR-GPU in this paper. We employ the SR-GPU implementation to perform the first phase of FH on a GPU. Note that the raster scan is decomposed into scans along each dimension of the image. The neighborhoods are defined as $N_G^{+,0}$ and $N_G^{0,+}$ for the sets of neighbors for the row-wise and column-wise scans, respectively. Similarly, for the anti-raster scan, $N_G^{-,0}$ and $N_G^{0,-}$ are defined for the respective axis-aligned component scans.

The transition from the raster scan phase to the wavefront propagation phase is slightly different from the sequential FH. The SR-GPU does not guarantee consistency when a pixel value is updated in parallel. Therefore, after the raster scan phase, pixels inserted into the queue for computation in the next phase are not only those from the anti-raster neighborhood (N_G^-) as in the sequential

Algorithm 5 Fast Parallel Hybrid Reconstruction

Input*I: mask image**J: marker image, defined on domain D_I , $J \leq I$.*

```
1: {Initialization phase}
2: Scan  $D_I$  in raster order.
3: for all  $rows \in D_I$  do in parallel
4:   Let  $p$  be the current pixel
5:    $J(p) \leftarrow (\max\{J(q), q \in N_G^{+,0}(p) \cup \{p\}\}) \wedge I(p)$ 
6: for all  $columns \in D_I$  do in parallel
7:   Let  $p$  be the current pixel
8:    $J(p) \leftarrow (\max\{J(q), q \in N_G^{0,+}(p) \cup \{p\}\}) \wedge I(p)$ 
9: Scan  $D_I$  in anti-raster order.
10: for all  $rows \in D_I$  do in parallel
11:   Let  $p$  be the current pixel
12:    $J(p) \leftarrow (\max\{J(q), q \in N_G^{-,0}(p) \cup \{p\}\}) \wedge I(p)$ 
13: for all  $columns \in D_I$  do in parallel
14:   Let  $p$  be the current pixel
15:    $J(p) \leftarrow (\max\{J(q), q \in N_G^{0,-}(p) \cup \{p\}\}) \wedge I(p)$ 
16: for all  $p \in D_I$  do in parallel
17:   if  $\exists q \in N_G(p) \mid J(q) < J(p)$  and  $J(q) < I(q)$ 
18:     queue_add(p)
19: {Wavefront propagation phase}
20: while queue_empty() = false do
21:   for all  $p \in queue$  do in parallel
22:     for all  $q \in N_G(p)$  do in parallel
23:       if  $J(q) < J(p)$  and  $I(q) \neq J(q)$  then
24:          $oldval = atomicMax(\&J(q), \min\{J(p), I(q)\})$ 
25:         if  $oldval < \min\{J(p), I(q)\}$  then
26:           queue.add(q)
```

algorithm, but also pixels from the entire neighborhood (N_G) satisfying the propagation condition (See Algorithm 5, Lines 16–18).

When two queued pixels (e.g., p' and p'') are computed in parallel, it is possible that they have common neighbors ($N_G(p') \cap N_G(p'') \neq \emptyset$). This can potentially create a race condition when updating the same neighbor q . Updating the value of a pixel q is done via a maximum operation, which can be efficiently implemented to avoid race conditions by employing atomic *Compare-and-Swap* (CAS) based instructions (*atomicMax* for GPUs). The value of pixel q before the update (*oldval*) is returned, which is used in our algorithm to test if q was updated due to the computation of the current pixel p' . If the *oldval* is not smaller than $\min\{J(p'), I(q)\}$, it indicates that the processing of another pixel p'' updated the value of q to a value greater than or equal to $\min\{J(p'), I(q)\}$. In this case, q has already been queued due to the p'' computation and does not need to be queued again. Otherwise, q is queued for computation. The overall process continues until the queue is empty. Note that the update operation is a maximum, hence an *atomicMax* is used instead of the *atomicCAS* operation in the generic wavefront propagation skeleton. It leads to better performance as the repeat-until loop in Algorithm 4 (Lines 5–14) is avoided. We also refer the reader to a previous technical report [46] with additional details on our GPU-based implementation of the Morphological Reconstruction.

3.4. GPU-enabled Euclidean Distance Transform

The GPU implementation of distance transform is shown in Algorithm 6. The implementation is very similar to the sequential version. The initialization phase assigns initial value to the Voronoi diagram and adds contour pixels or those background pixels with foreground neighbors for propagation (Lines 2 to 5).

In the wavefront propagation phase, for each pixel p queued for computation, its neighbor pixels q are checked to verify if using $VR(p)$ as path to a background pixel would result in a shorter distance as compared to the current path stored in $VR(q)$. If it does, $VR(q)$ is updated and q is queued for computation. Once again, concurrent computation of pixels in the queue may create a race condition if multiple threads try to update the same $VR(q)$. To prevent this condition, a compare and swap operation is employed when updating VR . VR is only updated if the value used to calculate distance (*curVRQ*) is still the value stored in $VR(q)$. Otherwise, the algorithm reads the new value stored in $VR(q)$ and calculates the distance again (Line 12). The final step, as in the sequential case, computes the distance map from VR . It is performed in parallel for all points in the input image.

A given VR diagram may have multiple valid solutions. If two pixels, p' and p'' , are equidistant and the closest background pixels to a foreground pixel q , either of the pixels can be used as the closest background pixel of q ($VR(q) = p'$ or $VR(q) = p''$). In other words, a foreground pixel could initially be assigned one of multiple background pixels, as long as the distance from the foreground pixel to those background pixels is the same. In our algorithm, the order in which the wave propagations are computed defines whether p' or p'' are used

Algorithm 6 Distance Transform Algorithm for GPUs

Input: I : mask image

Output: M : distance map image

FG : Foreground; BG : Background

```
1: {Initialization phase}
2: for all  $p \in D_I$  do in parallel
3:    $VR(p) = (I(p) == BG) ? p : inf$ 
4:   if  $I(p) == BG$  and  $\exists q \in N_G(p) \mid I(q) == FG$ 
5:     queue.add(p)
6: {Wavefront propagation phase}
7: while queue.empty() = false do
8:   for all  $p \in queue$  do in parallel
9:     for all  $q \in N_G(p)$  do
10:      repeat
11:         $curVRQ = VR(q)$ 
12:        if  $DIST(q, VR(p)) < DIST(q, curVRQ)$  then
13:           $old = atomicCAS(&VR(q), curVRQ, VR(p))$ 
14:          if  $old \neq curVRQ$  then
15:            queue.add(q)
16:            break;
17:          else
18:            break
19:        until True
20:      for all  $p \in D_I$  do in parallel
21:         $M(p) = DIST(p, VR(p))$ 
```

in such a case. However, since both pixels are equidistant to q , using either of them would result in the same distance map. Thus, the results achieved by the parallel distance transform are the same as those of the sequential version of the algorithm.

4. Parallel Execution on Multiple GPUs and CPUs

Our parallelization strategy, shown in Figure 5, for multiple GPUs and CPUs divides the input data domain into non-overlapping partitions (tiles). Local waveform propagations are computed independently for each partition. After the local propagations are computed, border information is exchanged to allow for inter-partition propagations. This process continues until there are no more propagations within a partition and between partitions.

Inter-processor communication is necessary because the irregular waveform propagation pattern involves waveform propagations that are data dependent. The shape of the waveform and the amount of wave propagation cannot be estimated prior to execution. As a result, a partitioning of the input data domain across processing units can incur inter-partition propagations and inter-processor communication, which cannot be eliminated by padding each domain partition.

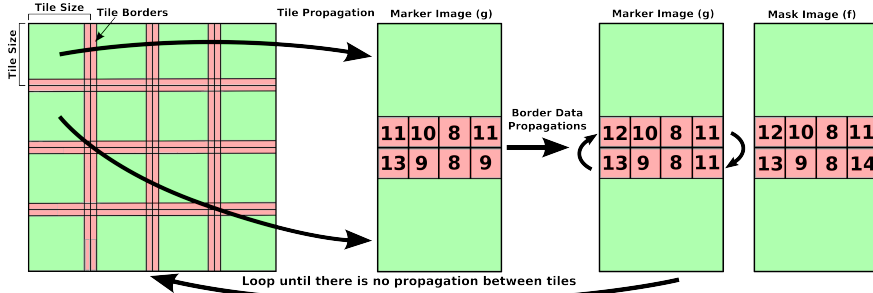


Figure 5: Tiling based parallelization (tiles are not necessarily square).

Figure 6 shows an example in which an input data domain is partitioned between two processors. The morphological reconstruction algorithm is used in this example. The input data domain, described in a 1-dimensional space in the example, is equally divided between processors 1 and 2 without any replication at the beginning of the execution (Figure 6(a)). Each processor independently performs the waveform propagation in their respective partitions by identifying seeds and computing the usual propagation as required by the algorithm. When the stability is reached (i.e., the queue is empty) in the partitions, there may be propagations crossing partition boundaries that have not been computed. Figure 6(b) presents the result of propagations within a partition. To compute inter-partition propagation effects correctly, processors must exchange border information to identify inter-partition propagations. After border information is exchanged, propagations originating from partition borders are initialized,

and another round of local propagations is executed. The process of performing local propagations and exchanging border information continues until no more propagations are possible within and between partitions. The final result of the morphological reconstruction for the 1-dimensional example is presented in Figure 6(c). The area recomputed because of the inter-partition propagations is represented in dark green.

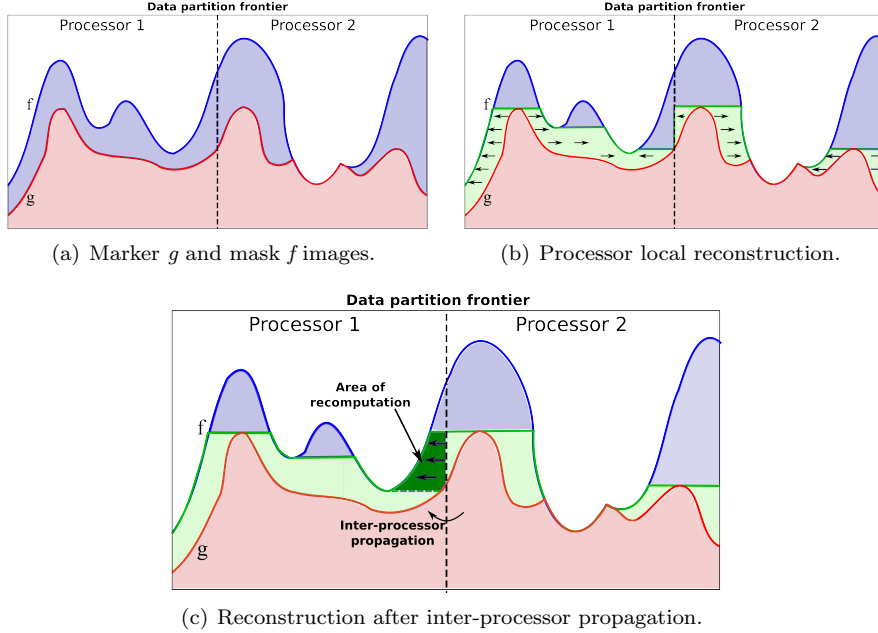


Figure 6: Evaluating Scalability According to the Number of Blocks.

The parallel implementation consists of a pipeline of two stages (Figure 7): Tile Propagation (TP) and Border Propagation (BP). The TP stage performs local propagations in tiles. An instance of this stage is created for each tile. The BP stage, on the other hand, computes propagations from data elements at tile borders. In essence, BP transmits propagations from one tile to another. When there is a need for propagation between tiles, BP will re-instantiate the pipeline. In that case, a TP instance is created for each tile receiving propagation and scheduled for execution. It computes propagations within the tile that are initiated from the borders. A new instance of BP is also created with a dependency on the new TP instances. That is, it is not scheduled for execution until all of the new TP instances finish their propagation computations. This cycle is repeated until there are no more intra-tile and inter-tile propagations.

The instances of the two stages are dispatched for execution on available CPUs and GPUs, as long as a stage has an implementation for those devices. We employ the concept of function variant, which is a group of functions with same name, arguments, and result types [25, 29]. In our implementation a function variant for a task is the CPU and GPU implementations of the operation.

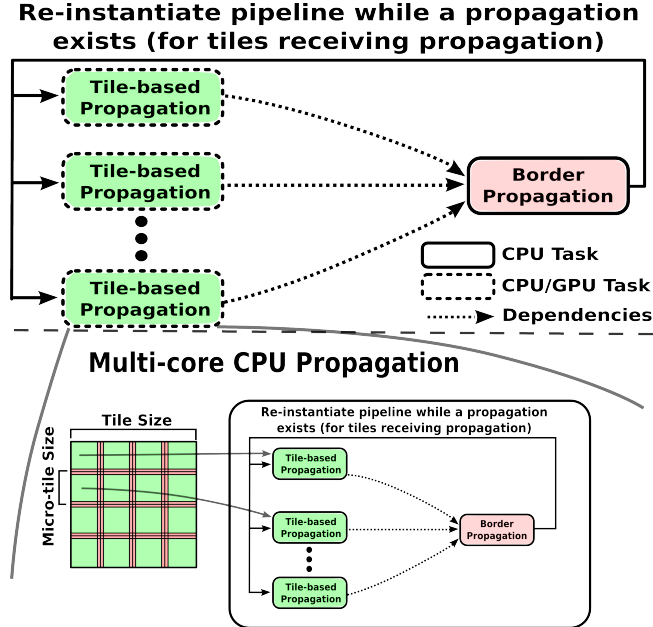


Figure 7: Pipeline representation of the CPU-GPU waveform propagation. Instances of Tile-based Propagation (TP) compute propagation in each tile as shown at the top. A Border Propagation (BP) stage, which depends on TP instances for execution, is also created to resolve propagation among the tiles. If a propagation exists between tiles, BP re-instantiates the pipeline. This process continues until stability is reached. The multi-level tiling strategy, in which a tile is repartitioned into micro-tiles for multi-core execution, is shown at the bottom. This strategy is implemented to reduce CPU vs GPU computational load imbalance.

Binding to a function variant enables the runtime system to choose the appropriate function or functions during execution, allowing multiple computing devices to be used concurrently and in a coordinated manner. We should note that a function variant provides opportunities for runtime optimizations, but an application is not required to provide CPU and GPU implementations for all of the stages.

Figure 8 presents an overview of our system support [47, 45] to schedule pipeline applications in machines equipped with multiple CPUs and GPUs. Tasks (TP and BP instances) dispatched for execution by the waveform propagation pipeline are either queued as ready to execute or inserted in a queue of pending tasks, respectively, depending on whether their dependencies are resolved or not. Tasks ready for execution are consumed by computing threads responsible for managing CPU cores and GPUs. A computing thread is assigned to each CPU-core or GPU available in the default mode. Assignment of tasks to computing devices is done in a demand-driven manner. When a CPU core or GPU remains idle, one of the tasks is assigned to the idle device. The default scheduling policy for choosing the task to be executed into a device requesting work is FCFS (first come, first served). In the case of our application, since the BP instance will be dependent on all TP instances, the BP is only dispatched

for execution after all the TPs have finished the execution.

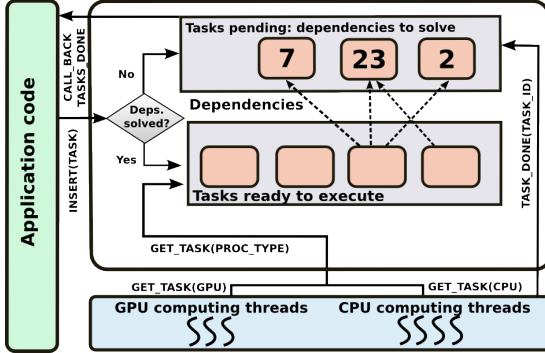


Figure 8: System support for execution of pipeline of tasks in machines equipped with multi-core CPUs and GPUs.

When a TP instance is scheduled for GPU execution, the tile to be processed is copied to the GPU memory. The results are transferred back to the CPU memory at the end of the processing. TP instances are dynamically assigned to processing devices using a demand-driven approach to alleviate load imbalance that may exist due to different computation requirements among tiles. Moreover, with a partitioning of input data into tiles, GPUs can be used when the input data does not fit into GPU memory as long as individual tiles do.

Our experimental evaluation showed that the maximum GPU performance for the IWPP is achieved when large input domain partitions are used. This is also observed for other types of GPU computations as larger inputs usually lead to higher computation times than better offset overheads of using GPUs. However, when CPUs and GPUs are used together, large tiles tend to reduce the performance gain because of the greater gap in execution times on a CPU core vs on a GPU. This increases load imbalance between the CPU and the GPU. To reduce the impact of load imbalance, our implementation allows for parallel CPU processing variants to be used. In this approach, instead of scheduling a single partition per CPU core, a single partition is scheduled to a group of CPU cores, if a parallel variant of the CPU processing operation is available. Consequently, a partition assigned to a CPU will have an execution time closer to that of a partition assigned to a GPU.

In the waveform propagation pattern, as presented on the bottom in Figure 7, a partition assigned for parallel CPU computation is broken into smaller micro-partitions that are processed by multiple CPU cores in parallel. Border communication between partitions assigned to different CPU cores is performed for inter-partition propagations. The runtime system (Figure 8) is responsible for setting the number of CPU cores available for a given partition. The multi-core version of the propagation stages is implemented on top of OpenMP [10].

5. Experimental Results

We evaluate the performance of the irregular wavefront propagation implementation using the morphological reconstruction and distance transform operations. These operations were applied on high-resolution RGB images from datasets collected by research studies in the In Silico Brain Tumor Research Center (ISBTRC) [39] at Emory University. The experiments were carried out on a machine (a single computation node of the Keeneland cluster [52]) with Intel® Xeon® X5660 2.8 GHz CPUs, 3 NVIDIA Tesla M2090 (Fermi) GPUs, and 24GB of DDR3 RAM (See Figure 9). A total of 12 CPU computing cores available because hyper-threading mechanism is not enabled. Codes used in our evaluation were compiled with “gcc 4.2.1”, “-O3” optimization flag, and NVidia CUDA SDK 4.0. The experiments were repeated 3 times, and, unless stated, the standard deviation was not observed to be higher than 1%. The speedup values presented in the following sections are calculated based on the performance of single CPU-core versions of the operations.

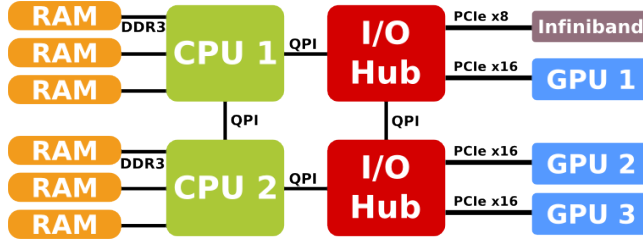


Figure 9: Hybrid, Multi-GPU computing node.

5.1. Multi-core CPU Parallelization

Two different multi-core CPU parallelization strategies were implemented on top of OpenMP: (i) *Tile-based parallelization* that partitions an input image into regions and iteratively solves propagations local to each partition and performs inter-region propagations, as described in Section 4; (ii) *Non-Tiled parallelization* is an alternative parallelization in which points in the initial wavefront are distributed in round-robin among CPU threads at the beginning of the execution. Each thread then independently computes propagations associated with the points assigned to it. To avoid inter-thread interference in propagations, it is necessary to use *atomic* compare-and-swap operations during data updates.

The performances of both parallelization strategies are presented in Figure 10. The non-tiled parallelization of the morphological reconstruction resulted in slowdown as compared to the sequential algorithm for most of the configurations; only a slight improvement was observed on 8 CPU cores. In order to understand this poor performance, the algorithm was profiled using *perf* profiling tool [21] to measure the effects of increasing number of threads to cache and bus cycles. Additional bus cycles are used for data read and write as

well as for data transfers to assert cache coherence among threads. An increase in the number of threads from 1 to 2 in the non-tiled parallelization results in twice more cache misses and three times more bus cycles. Similar behavior is observed as the number of threads keep increasing, preventing the algorithm from having gains as more CPU cores are used. For this parallelization, threads may be concurrently computing in the same region of the input domain, and updates from one thread will invalidate cache lines of all the other threads processing the same region. This makes the cost of maintaining cache coherence very high.

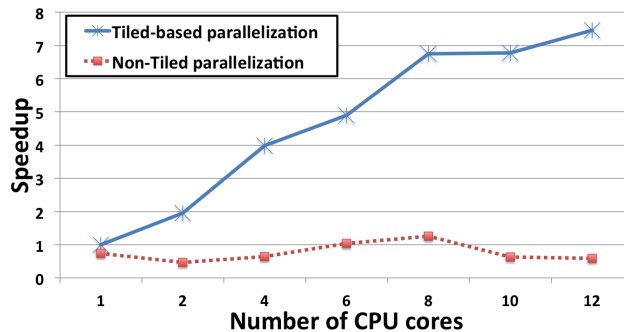


Figure 10: Multicore performance of morphological reconstruction. Different parallelization strategies are compared.

The performance of the tile-based parallelization is much better with a speedup of $7.5\times$ in the configuration with 12 threads. This is a result of avoiding inter-thread interference. Because threads are assigned to independent partitions, they do not modify the same regions and affect each other. Nevertheless, the speedup performance of the algorithm is sub-linear. This is an inevitable consequence of the threads’ having to share the processor cache space and the bus subsystem. Since the algorithm is very data intensive, larger cache and fast access to memory are primordial to achieve maximum performance, and contention on these resources limits gains in CPU multicore systems.

5.2. GPU Parallelization

The experiments in this section examine the impact on performance of the queue design as well as tile size and input data characteristics for the GPU-enabled implementations of irregular wavefront propagation computations.

5.2.1. Impact of Queue Design Choices

This set of experiments evaluates the performance of three different parallel queue approaches: (i) Naïve. This is the simple queue implementation based on the atomic add operations only; (ii) Prefix-sum (PF). PF performs a prefix-sum among GPU threads to calculate the positions where items are stored in the queue, reducing the synchronization cost due to the atomic operations; and, (iii) Prefix-sum + Per-Thread Queue (TQ). TQ employs local queues in

addition to the prefix-sum optimization in order to reduce the number of prefix-sum/synchronization phases. In the experiments we present results from the morphological reconstruction implementation – there is no significant difference between these results and those from the distance transform implementation.

The different queue versions are compared using a 4-connected grid and a $4K \times 4K$ input image tile with 100% of tissue coverage. As a strategy to initialize the queue with different number of pixels and evaluate its performance under various scenarios, the number of raster and anti-raster scans performed in the initialization is varied. A single thread block is created per Stream Multiprocessor (SM) of the GPU. The execution times reported in Table 1 correspond to the wavefront phase only.

Initial	Total	#Raster Scans	Naïve	PF	TQ
534K	30.4M	7	685	291	228
388K	22.2M	9	527	223	175
282K	16.7M	11	409	164	134
210K	12.7M	13	323	133	106
158K	9.9M	15	255	118	98
124K	7.7M	17	207	99	83
97K	6.2M	19	162	84	70

Table 1: Execution times in milliseconds (ms) for different versions of the queue: Naïve, Prefix-sum (PF), and Prefix-sum + Per-Thread Queue (TQ). The columns Initial and Total indicate the number of pixels initially queued before the wavefront propagation phase is executed and the total number of pixels queued/dequeued during the execution, respectively.

The results show that the Naïve queue has the highest execution times in all the experiments. The PF implementation was on average able to improve the performance compared to Naïve version by $2.31\times$. These performance improvements indicate that atomic operations, while they are much faster in modern GPUs [31], still introduce significant overhead and that the heavy use of atomic operations should be considered carefully. The results in the table also show that TQ, which uses local queues to further reduce synchronization, achieved performance improvements of $1.24\times$ on top of PF. These gains with the different versions of the queue demonstrate the benefits of employing prefix-sum to reduce the number of atomic operations and local queues to minimize synchronization among threads.

5.2.2. Effects of Tile Size

The experiments in this section evaluate the impact of the tile size to the performance of the morphological reconstruction and distance transform algorithms. Figure 11 presents the morphological reconstruction algorithm performance using an 8-connected G grid and an input image of $64K \times 64K$ pixels with 100% tissue coverage. Two versions of this algorithm were evaluated: FH_GPU that is implemented using the irregular wavefront propagation framework; and, SR_GPU [20] that is based on raster and anti-raster scans. SR_GPU was the fastest GPU implementation of morphological reconstruction available before

our work. All speedup values are calculated using the single core CPU version of the application as reference.

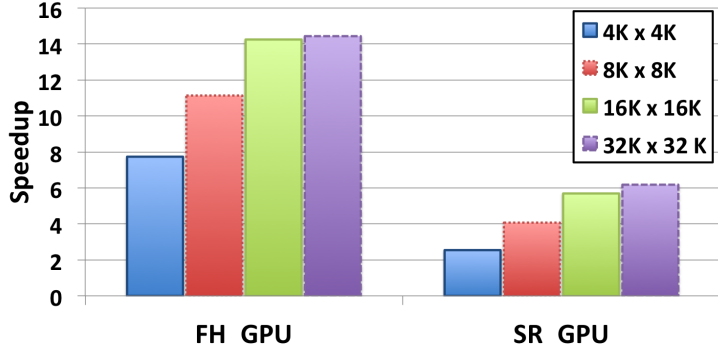


Figure 11: Morphological Reconstruction: performance of the IWPP based implementation (FH_GPU) and Pavas algorithm [20] (SR_GPU) that is implemented as iterative raster scanning according to the input data tile size.

The results show that the performances of both GPU algorithms improve as the tile size is increased until $16K \times 16K$ pixels; beyond this size no significant additional gains are observed. The better speedup values with larger tiles are the result of (i) better amortization of initialization of computations with the GPU, specially in the raster scan pass (SR_GPU and the initialization phase of FH_GPU), which launches four GPU *kernels* per iteration; and (ii) the larger amount of parallelism available with big tiles. The experimental results show that FH_GPU performs better than SR_GPU [20] in all the configurations, on average about $2.6\times$ better. Further, FH_GPU achieves a performance improvement of $14.3\times$ compared to the single core CPU version. It is important to highlight, however, that the FH_GPU is a two phase algorithm that includes raster scans in the initialization phase. The initial scan is responsible for about 43% of the execution time, reducing performance gains from the wavefront propagation phase.

Tile Size	$4K \times 4K$	$8K \times 8K$	$16K \times 16K$	$32K \times 32K$
Speedup	31.4	36.8	37.5	37.1

Table 2: Distance Transform: performance according to the input data tile size.

The performance of the distance transform implementation is presented in Table 2. The initialization phase in this algorithm is inexpensive. Most of the execution time is spent in the wavefront propagation phase, which is less sensitive to the tile size because of its lower overheads – all of the computation in this phase is performed within a single GPU *kernel*, while in the raster scanning phase 4 *kernel* calls are executed per pass on the image.

5.2.3. Impact of Input Data Characteristics

These experiments employed four different images with $64K \times 64K$ pixels, shown in Figure 12, that have different percentage of tissue coverage. The 25%, 50%, 75%, and 100% of the image area is covered with tissue (in contrast to background) in images 1, 2, 3, and 4, respectively. The images are partitioned into tiles of size $16K \times 16K$ to fit into the GPU memory. Inter-partition propagations are performed as discussed in Section 4.

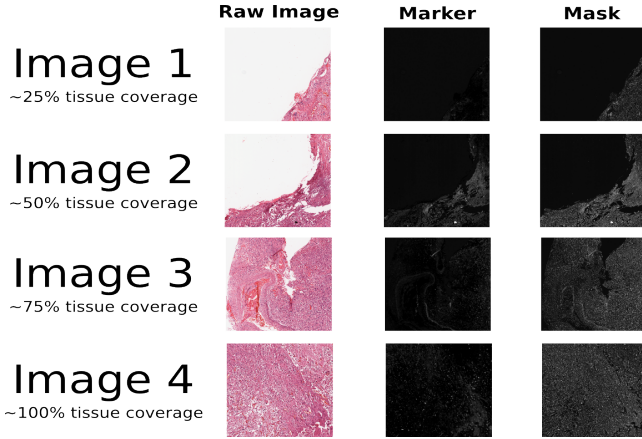


Figure 12: Raw image, marker, and mask for tiles with different amount of tissue coverage.

The speedup values of FH_GPU and SR_GPU with respect to the single core CPU version are presented in Figure 13. The performances of the GPU implementations get better with images with larger tissue coverage. Larger tissue coverage implies more work that can be done in parallel, which amortizes the overhead of starting the GPU computations. In addition, the higher parallelism for images with larger tissue coverage increases the utilization of GPU threads and reduces the chances of having conflicting atomic operations between threads.

The comparison of FH_GPU and SR_GPU shows a consistent performance gap between the implementations for all variations of the input images. In our experiments, FH_GPU achieved performance improvements of up to $3.1 \times$ on top of SR_GPU. The performance gains of FH_GPU are higher for images with less tissue coverage. For those images, SR_GPU passes over the entire input image domain irrespective of the number of pixels being modified, resulting in more unnecessary computation that does not contribute to the output.

The performance of the distance transform implementation as the input data is varied is presented in Figure 14. As in the morphological reconstruction implementation, larger tissue coverage results in higher speedup values. Once again, this is a consequence of more computation and parallelism available with images with more tissue coverage. More tissue coverage means there are more foreground pixels from which to calculate distances to a background pixel.

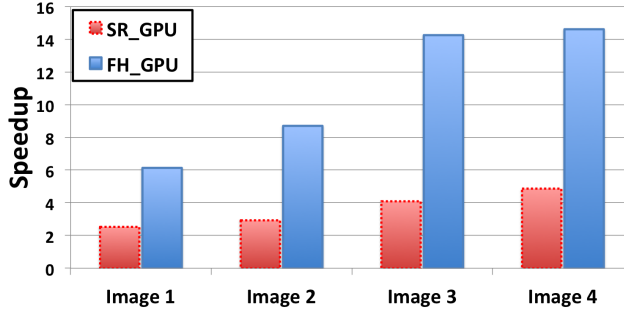


Figure 13: Performance variation of the morphological reconstruction implementation with respect to input data characteristics.

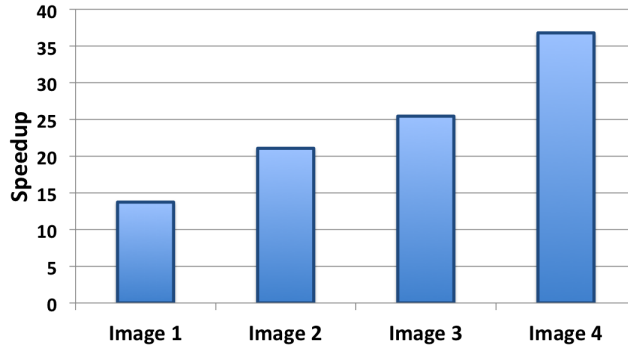


Figure 14: Performance variation of the distance transform implementation with respect to input data characteristics.

5.2.4. Impact of Exceeding Queue Storage Limit

This set of experiments vary the memory space available for the queue to store pixels. When the queue storage limit is exceeded, our implementation throws away excess pixels. Then it is necessary to perform another round of computations to compute any missing wavefront propagations. To stress the algorithm, we reduced the space available for the queue until we created two scenarios. In the first scenario, the queue storage limit is exceeded once, and the wavefront propagation execution phase has to be re-launched to fix any missing propagations. In the second scenario, the queue storage limit is exceeded in the second iteration of the wavefront propagation phase as well. As a result, a third iteration of this phase is needed to finish computation correctly.

The experimental results were obtained using the morphological reconstruction implementation and a single input tile of $4K \times 4K$ pixels. The results show that performance penalty due to exceeding the queue storage limit is small. For instance, the performance hit is 6% when the queue is exceeded once during the

execution and 9% when it is exceeded twice. In general, we observed that setting a storage limit that is 10% larger than the initial queue size was sufficient.

5.3. Cooperative Multi-GPU Multi-CPU Execution

These experiments evaluate the implementations when multiple GPUs and CPUs are used cooperatively for execution. The input images have 100% tissue coverage. The resolutions of the images are $96K \times 96K$ pixels and $64K \times 64K$ pixels for the morphological reconstruction implementation and the distance transform implementation, respectively; these are the maximum size images that can fit in the main CPU memory for each algorithm.

The multi-GPU scalability of the morphological reconstruction algorithm is presented in Figure 15(a). The speedups achieved for one, two, and three GPUs, in comparison to the CPU single core version, are about $16\times$, $30\times$ and $43\times$. The overall performance improvement is good, but the 3-GPUs execution achieves $2.67\times$ speedup with respect to the 1-GPU version which is below linear. To investigate the reasons, we calculated the average cost of the wavefront propagation phase by breaking it down into three categories: (i) *Computation*, which is the time spent by the application *kernels*; (ii) *Download*, which corresponds to the time to download the results from GPU to CPU memory; and (iii) *Upload*, which includes data copy from CPU to GPU. The results, presented in Figure 15(b), show that there is an increase in data transfer costs as more GPUs are used, limiting the scalability. We should note that we efficiently utilized the architecture of the node, which is built with two I/O Hubs connecting CPUs to GPUs (see Figure 9). In our approach, the CPU thread managing a GPU is mapped to a CPU closer to the corresponding GPU. This allows for maximum performance to be attained during data transfers. When this placement is not employed, the performance of the multi-GPU scalability is degraded and only small performance improvements are observed when more than two GPUs are utilized.

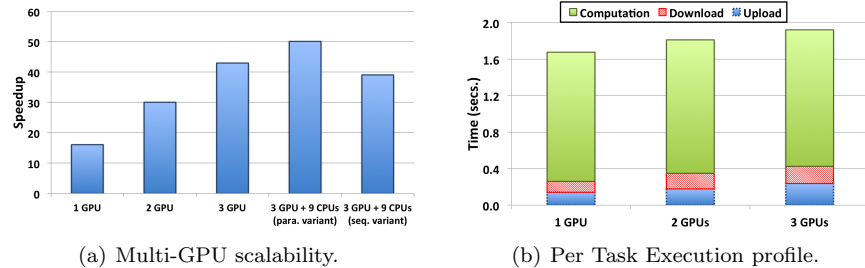


Figure 15: Performance of the morphological reconstruction implementation on multiple GPUs and using multiple CPUs and GPUs together.

Figure 15(a) also presents the cooperative CPU–GPU execution performance. In this scenario, when the multi-core version of the CPU operation

is used (parallel variant), the multi-CPU multi-GPU executions achieve extra performance improvements of about $1.17\times$ with respect to the 3-GPU configuration, or a total of $50\times$ speedup on top of the single core CPU execution. As is shown in the figure, the use of sequential CPU variants results in performance loss with respect to the multi-GPU only execution. This performance degradation is the result of load imbalance among devices, which is higher with the sequential variants due to the larger gap in execution times between a GPU execution and a single CPU core. The computation time for the $96K \times 96K$ pixel image in the cooperative execution mode using all the CPUs and GPUs was 21 seconds.

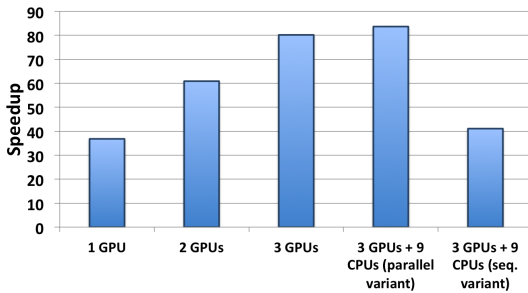


Figure 16: Performance of the distance transform implementation on multiple GPUs and using multiple CPUs and GPUs together.

Finally, Figure 16 presents the cooperative multi-GPU/-CPU execution results for distance transform. Similar to that of the morphological reconstruction implementation, the multi-GPU scalability is good, but it is sub-linear because of increasing data transfer costs. The cooperative CPU—GPU execution, in this case, resulted in a speedup of $1.07\times$ on top of the execution with 3 GPUs. The smaller improvement percentage, as compared to the morphological reconstruction algorithm, is simply because of the better GPU acceleration achieved by distance transform. The overall speedups of the algorithm when all GPUs and CPU cores are employed together is about $85.6\times$, as compared to the single CPU core execution. For reference, the distance transform computation on the $64K \times 64K$ pixel image took only 4.1 seconds.

6. Related work

The irregular wavefront propagation pattern has similarities to some fundamental graph scan algorithms, such as Breadth-First Search (BFS), but modified to support multiple sources. Much effort has been put into the development of parallel implementations of BFS on multi-core CPUs [1] and GPUs [17, 27]. The GPU implementation proposed in [27] is based on a sequence of iterations until all nodes are visited. Each iteration visits all nodes on the graph and

processes those that are on the propagation frontier. The work by Hong et al. [17] targeted new techniques to avoid load imbalance when nodes in a graph have a highly irregular distribution of degrees (number of edges per node). In image operations with IWPP the approach proposed by Hong et al. would not do any better than what was suggested by Karas [20], since the degree of all nodes (pixels) is the same and defined by the structuring element G . Moreover, the irregular wavefront propagation based approach visits those nodes (data elements) that are modified – i.e., queued in the last iteration –, instead of all the nodes to compute only those that are in the frontier as in [17].

The queue in our case is heavily employed and hundreds of thousands to millions of nodes (pixels) may be queued per iteration. The solution introduced in earlier work [27], if employed in the IWPP, would require expensive inter-block communication at each iteration of the application. This synchronization is realized by synchronizing all thread blocks, stopping the *kernel* execution, and re-launching another round of computation. Unlike the previous work [27], we propose that a scalable hierarchical queue be employed in a per-block basis. This avoids communication among blocks and permits the entire computation to be efficiently carried out into a single *kernel* call. Moreover, since the connectivity of a pixel is known a priori, we can employ local queues more aggressively to provide very fast local storage, as well as use parallel prefix-sum based reductions to avoid expensive atomic operations when storing items into the queue. Additionally, in our solution, an arbitrary large number of blocks may be used, which enables the implementation to leverage GPU’s dynamic block scheduler in order to alleviate the effects of inter-block load imbalance.

Various image processing algorithms have been ported to GPUs for efficient execution [14, 22, 41]. In addition, there is a growing set of libraries, such as the NVIDIA Performance Primitives (NPP) [32] and OpenCV [5], which encapsulate GPU-implementations of a number of image processing algorithms through high level and flexible APIs. Most of the algorithms currently available with this APIs, however, have more regular computation patterns as compared to IWPP.

Morphological reconstruction has been increasingly employed by several applications in the last decade. Efficient algorithms [55, 24] and a number of applications were presented by Vincent [53]. Other variants of Vincent’s fast hybrid algorithm (FH) have been proposed, such as the downhill filter approach [35]. We have tested this approach on our datasets and found it to be slower than FH. The high computational demands of morphological reconstruction motivated other works that employed specialized processors to speedup this algorithm. Jivet et al. [19] implemented a version using FPGAs, while Karas et al. [20] targeted GPUs. In both cases, however, the parallel algorithms were designed on top of a sequential baseline version that is intrinsically parallelizable, but about one order of magnitude slower than the fastest sequential version. In our solution, on the other hand, we extend the fastest baseline algorithm which exhibits the irregular wavefront propagation pattern. This approach has resulted in strong and consistent performance improvements on top of the existing GPU implementation by Karas [20].

Euclidean distance transform is also important in image analysis and used in several tasks as watershed based segmentation. This algorithm is very compute demanding, which has attracted considerable attention in the last few years regarding strategies for GPU acceleration [37, 36, 40, 7]. Among the proposed solutions, the work of Schneider et al. [40] is the most similar to our distance transform algorithm, because it also implements an output that is equivalent to that of Danielsson’s distance transform [11]. This GPU implementation, however, is based on sweeps over the entire dataset, instead of using propagations that process only those elements in the wavefront as in our case. Moreover Schneider’s algorithm only performs propagation of pixels in one row at time, considering 2D problems, which limits GPU utilization. Unfortunately, this code is not available for comparison, but the levels of acceleration achieved in our case are higher than what Schneider’s algorithm attained. No multi-CPU multi-GPU algorithms have been developed for morphological reconstruction and euclidean distance transform in the previous works.

The use of CPUs and GPUs cooperatively has gained attention of the research community in the last few years. Several works have developed system and compiler techniques to support efficient execution on heterogeneous CPU-GPU equipped machines [25, 26, 48, 43, 44, 4, 34, 18, 16]. In this paper, differently from previous work, we present a domain specific framework for parallelization of irregular wavefront propagation based applications in CPU-GPU equipped machines. This framework leverages the computation power of such environments to a large class of applications by exporting a high level set of tools, which may be used by a programmer to accelerate applications fitting in the irregular wavefront propagation pattern.

7. Conclusions

The efficiency of the *irregular wavefront propagation pattern* relies on tracking points in the wavefront and, consequently, avoiding unnecessary computation to visit and process parts of the domain that do not contribute to the output. This characteristic of the IWPP makes it an efficient computation structure in image analysis and other applications [55, 53, 56, 28, 23, 54, 33, 15, 51]. Nevertheless, the parallelization of the IWPP on hybrid systems with multi-core CPUs and GPUs is complicated because of the dynamic, irregular, and data dependent data access and processing pattern. Our work has showed that a multi-level queue to track the wavefronts provides an efficient data structure for execution on a GPU. The multi-level queue structure enables the efficient use of fast memory hierarchies on a GPU. Inter- and intra-thread block scalability can be achieved by per block queues and parallel prefix-sum index calculation to avoid heavy use of atomic operations.

We also have proposed a multi-processor execution strategy that divides the input domain into disjoint partitions (tiles) and assigns tiles to computing devices (CPU cores and GPUs) in a demand-driven fashion to reduce load imbalance. The tile based parallelization is critical to achieving scalability on multi-core systems, since it reduces inter-thread interferences because of computation

of the same regions of the domain without tiling. Inter-thread interferences cause inefficient use of cache.

In order to evaluate the proposed approaches we have developed IWPP-based implementations of two widely used image processing operations, morphological reconstruction and euclidean distance transform, on a state-of-the-art hybrid machine. In our experimental evaluation, these implementations have achieved orders of magnitude performance improvement (of upto $85\times$) over the sequential CPU versions. Our results showed that coordinated use of CPUs and GPUs makes it feasible to process high resolution images in reasonable times, opening the way for large scale imaging studies.

Limitations of the Current Work. This work focuses on the developing support for execution of the IWPP on shared memory hybrid machines equipped with multicore CPUs and GPUs. The current implementation does not support use of distributed multi-node machines. The parallelization strategy we employ for multiple GPUs and CPUs (Section 4), however, can be extended for the multi-node case. In this scenario, a messaging passing mechanism should be employed to exchange information necessary for propagations to cross partitions of the input domain assigned to different machines.

Acknowledgments. This research was funded, in part, by grants from the National Institutes of Health through contract HHSN261200800001E by the National Cancer Institute; and contracts 5R01LM009239-04 and 1R01LM011119-01 from the National Library of Medicine, R24HL085343 from the National Heart Lung and Blood Institute, NIH NIBIB BISTI P20EB000591, RC4MD005964 from National Institutes of Health, and PHS Grant UL1TR000454 from the Clinical and Translational Science Award Program, National Institutes of Health, National Center for Advancing Translational Sciences. This research used resources of the Keeneland Computing Facility at the Georgia Institute of Technology, which is supported by the National Science Foundation under Contract OCI-0910735. The content is solely the responsibility of the authors and does not necessarily represent the official views of the NIH. We also want to thank Pavel Karas for releasing the SR-GPU implementation used in our comparative evaluation.

References

- [1] V. Agarwal, F. Petrini, D. Pasetto, and D. A. Bader. Scalable Graph Exploration on Multicore Processors. In *Proceedings of the 2010 ACM/IEEE International Conference for High Performance Computing, Networking, Storage and Analysis*, SC ’10, 2010.
- [2] C. Ancourt and F. Irigoin. Scanning polyhedra with DO loops. In *Proceedings of the Third ACM SIGPLAN symposium on Principles and Practice of Parallel Programming*, PPOPP ’91, pages 39–50, New York, NY, USA, 1991. ACM.

- [3] U. Banerjee. Unimodular Transformation of Double Loops. In *Advances in Languages and Compilers for Parallel Computing*, pages 192–219, London, UK, 1991. Pitman Publishing.
- [4] G. Bosilca, A. Bouteiller, T. Herault, P. Lemarinier, N. Saengpatsa, S. Tomov, and J. Dongarra. Performance Portability of a GPU Enabled Factorization with the DAGuE Framework. In *2011 IEEE International Conference on Cluster Computing (CLUSTER)*, pages 395–402, sept. 2011.
- [5] G. Bradski. The OpenCV Library. *Dr. Dobb's Journal of Software Tools*, 2000.
- [6] I. Buck, T. Foley, D. Horn, J. Sugerman, K. Fatahalian, M. Houston, and P. Hanrahan. Brook for gpus: stream computing on graphics hardware. *ACM Trans. Graph.*, 23(3):777–786, 2004.
- [7] T.-T. Cao, K. Tang, A. Mohamed, and T.-S. Tan. Parallel Banding Algorithm to compute exact distance transform with the GPU. In *Proceedings of the 2010 ACM SIGGRAPH symposium on Interactive 3D Graphics and Games*, I3D ’10, pages 83–90, New York, NY, USA, 2010. ACM.
- [8] O. Cuisenaire and B. Macq. Fast euclidean distance transformation by propagation using multiple neighborhoods. *Computer Vision and Image Understanding*, 76(2):163 – 172, 1999.
- [9] R. da S. Torres, A. Falcao, and L. da F. Costa. A graph-based approach for multiscale shape analysis. *Pattern Recognition*, 37(6):1163 – 1174, 2004.
- [10] L. Dagum and R. Menon. OpenMP: an industry standard API for shared-memory programming. *IEEE Computational Science and Engineering*, 5(1):46–55, Jan-Mar 1998.
- [11] P.-E. Danielsson. Euclidean distance mapping. *Computer Graphics and Image Processing*, 14:227–248, 1980.
- [12] R. Fabbri, L. D. F. Costa, J. C. Torelli, and O. M. Bruno. 2D Euclidean distance transform algorithms: A comparative survey. *ACM Comput. Surv.*, 40(1):2:1–2:44, Feb. 2008.
- [13] A. X. Falcão, L. da Fontoura Costa, and B. S. S. D. Cunha. Multiscale skeletons by image foresting transform and its application to neuromorphometry. *Pattern Recognition*, 35(7):1571–1582, 2002.
- [14] O. Fialka and M. Cadik. FFT and Convolution Performance in Image Filtering on GPU. In *Proceedings of the conference on Information Visualization*, pages 609–614, 2006.
- [15] R. K. Gabriel and R. R. Sokal. A New Statistical Approach to Geographic Variation Analysis. *Systematic Zoology*, 18(3):259–278, Sept. 1969.

- [16] T. D. Hartley, U. V. Catalyurek, A. Ruiz, M. Ujaldon, F. Igual, and R. Mayo. Biomedical image analysis on a cooperative cluster of gpus and multicores. In *22nd ACM Intl. Conference on Supercomputing*, Dec 2008.
- [17] S. Hong, S. K. Kim, T. Oguntebi, and K. Olukotun. Accelerating CUDA graph algorithms at maximum warp. In *Proceedings of the 16th ACM symposium on Principles and Practice of Parallel Programming*, PPoPP '11, pages 267–276. ACM, 2011.
- [18] X. Huo, V. Ravi, and G. Agrawal. Porting irregular reductions on heterogeneous cpu-gpu configurations. In *18th International Conference on High Performance Computing (HiPC)*, pages 1–10, dec. 2011.
- [19] I. Jivet, A. Brindusescu, and I. Bogdanov. Image contrast enhancement using morphological decomposition by reconstruction. *WSEAS Trans. Cir. and Sys.*, 7:822–831, August 2008.
- [20] P. Karas. Efficient Computation of Morphological Greyscale Reconstruction. In *MEMICS*, volume 16 of *OASICs*, pages 54–61. Schloss Dagstuhl - Leibniz-Zentrum fuer Informatik, Germany, 2010.
- [21] L. Kernel. *Perf profiling tool*. GNU, 2012.
- [22] A. Körbes, G. B. Vitor, R. de Alencar Lotufo, and J. V. Ferreira. Advances on watershed processing on GPU architecture. In *Proceedings of the 10th International Conference on Mathematical Morphology*, ISMM'11, pages 260–271, 2011.
- [23] C. Lantuéjoul. Skeletonization in quantitative metallography. In R. Haralick and J.-C. Simon, editors, *Issues in Digital Image Processing*, volume 34 of *NATO ASI Series E*, pages 107–135, 1980.
- [24] C. Laurent and J. Roman. Parallel implementation of morphological connected operators based on irregular data structures. In *Third International Conference on Vector and Parallel Processing*, VECPAR '98, pages 579–592, London, UK, UK, 1999. Springer-Verlag.
- [25] M. D. Linderman, J. D. Collins, H. Wang, and T. H. Meng. Merge: a programming model for heterogeneous multi-core systems. *SIGPLAN Not.*, 43(3):287–296, 2008.
- [26] C.-K. Luk, S. Hong, and H. Kim. Qilin: Exploiting parallelism on heterogeneous multiprocessors with adaptive mapping. In *42nd International Symposium on Microarchitecture (MICRO)*, 2009.
- [27] L. Luo, M. Wong, and W.-m. Hwu. An effective GPU implementation of breadth-first search. In *Proceedings of the 47th Design Automation Conference*, DAC '10, pages 52–55, 2010.

- [28] F. Meyer. Digital Euclidean Skeletons. In *SPIE Vol. 1360, Visual Communications and Image Processing*, pages 251–262, 1990.
- [29] T. Millstein. Practical predicate dispatch. *SIGPLAN Not.*, 39:345–364, October 2004.
- [30] J. C. Mullikin. The vector distance transform in two and three dimensions. *CVGIP: Graphical Models and Image Processing*, 54(6):526 – 535, 1992.
- [31] Nvidia. *Fermi Compute Architecture Whitepaper*.
- [32] NVIDIA. *NVIDIA Performance Primitives(NPP)*, 11 February 2011.
- [33] F. P. Preparata and M. I. Shamos. *Computational geometry: an introduction*. Springer-Verlag New York, Inc., New York, NY, USA, 1985.
- [34] V. Ravi, W. Ma, D. Chiu, and G. Agrawal. Compiler and runtime support for enabling generalized reduction computations on heterogeneous parallel configurations. In *Proceedings of the 24th ACM International Conference on Supercomputing*, page 137146. ACM, 2010.
- [35] K. Robinson and P. F. Whelan. Efficient morphological reconstruction: a downhill filter. *Pattern Recogn. Lett.*, 25:1759–1767, November 2004.
- [36] G. Rong and T.-S. Tan. Jump flooding in GPU with applications to Voronoi diagram and distance transform. In *Proceedings of the 2006 symposium on Interactive 3D graphics and games*, I3D ’06, pages 109–116, 2006.
- [37] G. Rong and T.-S. Tan. Variants of Jump Flooding Algorithm for Computing Discrete Voronoi Diagrams. In *Proceedings of the 4th International Symposium on Voronoi Diagrams in Science and Engineering*, ISVD ’07, pages 176–181, 2007.
- [38] A. Rosenfeld and J. L. Pfaltz. Sequential operations in digital picture processing. *J. ACM*, 13(4):471–494, Oct. 1966.
- [39] J. H. Saltz and *et al.*. Multi-scale, integrative study of brain tumor: In silico brain tumor research center. In *Annual Symposium of American Medical Informatics Association 2010 Summit on Translational Bioinformatics (AMIA-TBI 2010)*, Mar 2010.
- [40] J. Schneider, M. Kraus, and R. Westermann. GPU-based Real-time Discrete Euclidean Distance Transforms with Precise Error Bounds. In A. Ranchordas and H. Araújo, editors, *VISAPP (1)*, pages 435–442. INSTICC Press, 2009.
- [41] I. Scholl, T. Aach, T. M. Deserno, and T. Kuhlen. Challenges of medical image processing. *Comput. Sci.*, 26:5–13, February 2011.

- [42] F. Y. Shih and Y.-T. W. Y.-T. Wu. The efficient algorithms for achieving euclidean distance transformation. *IEEE Transactions on Image Processing*, 13(8):1078–1091, 2004.
- [43] N. Sundaram, A. Raghunathan, and S. T. Chakradhar. A framework for efficient and scalable execution of domain-specific templates on GPUs. In *IPDPS '09: Proceedings of the 2009 IEEE International Symposium on Parallel and Distributed Processing*, pages 1–12, 2009.
- [44] G. Teodoro, T. D. R. Hartley, U. Catalyurek, and R. Ferreira. Run-time optimizations for replicated dataflows on heterogeneous environments. In *Proc. of the 19th ACM International Symposium on High Performance Distributed Computing (HPDC)*, 2010.
- [45] G. Teodoro, T. M. Kurc, T. Pan, L. A. Cooper, J. Kong, P. Widener, and J. H. Saltz. Accelerating Large Scale Image Analyses on Parallel, CPU-GPU Equipped Systems. In *IPDPS '12: Proceedings of the 2012 IEEE International Symposium on Parallel and Distributed Processing*, 2012.
- [46] G. Teodoro, T. Pan, T. M. Kurc, J. Kong, L. Cooper, and J. H. Saltz. A Fast Parallel Implementation of Queue-based Morphological Reconstruction using GPUs. Technical Report CCI-TR-2012-2, Emory University, Jan. 2012.
- [47] G. Teodoro, T. Pan, T. M. Kurc, J. Kong, L. Cooper, and J. H. Saltz. High-throughput Execution of Hierarchical Analysis Pipelines on Hybrid Cluster Platforms. Technical Report CCI-TR-2012-4, Emory University, May 2012.
- [48] G. Teodoro, R. Sachetto, O. Sertel, M. Gurcan, W. M. Jr., U. Catalyurek, and R. Ferreira. Coordinating the use of GPU and CPU for improving performance of compute intensive applications. In *IEEE Cluster*, 2009.
- [49] S. Tomov, R. Nath, H. Ltaief, and J. Dongarra. Dense Linear Algebra Solvers for Multicore with GPU Accelerators. *IPDPS '10: Proceedings of the 2010 IEEE International Symposium on Parallel and Distributed Processing*, 2010.
- [50] R. Torres, A. Falcao, and L. Costa. Shape description by image foresting transform. In *2002 14th International Conference on Digital Signal Processing, 2002. DSP 2002.*, volume 2, pages 1089 – 1092 vol.2, 2002.
- [51] G. T. Toussaint. The relative neighbourhood graph of a finite planar set. *Pattern Recognition*, 12(4):261–268, 1980.
- [52] J. S. Vetter, R. Glassbrook, J. Dongarra, K. Schwan, B. Loftis, S. McNally, J. Meredith, J. Rogers, P. Roth, K. Spafford, and S. Yalamanchili. Keeneland: Bringing heterogeneous gpu computing to the computational science community. *Computing in Science and Engineering*, 13, 2011.

- [53] L. Vincent. Exact Euclidean Distance Function By Chain Propagations. In *IEEE Int. Computer Vision and Pattern Recog. Conference*, pages 520–525, 1991.
- [54] L. Vincent. Morphological area openings and closings for grey-scale images. In *Proc. of the Workshop "Shape in Picture"*, pages 197–208. Springer, 1992.
- [55] L. Vincent. Morphological grayscale reconstruction in image analysis: Applications and efficient algorithms. *IEEE Transactions on Image Processing*, 2:176–201, 1993.
- [56] L. Vincent and P. Soille. Watersheds in Digital Spaces: An Efficient Algorithm Based on Immersion Simulations. *IEEE Transactions on Pattern Analysis and Machine Intelligence*, 13(6):583–598, June 1991.
- [57] M. Wolfe. Loops skewing: The wavefront method revisited. *International Journal of Parallel Programming*, 15:279–293, 1986. 10.1007/BF01407876.
- [58] S. Xiao and W. chun Feng. Inter-block GPU communication via fast barrier synchronization. In *IPDPS '10: Proceedings of the 2010 IEEE International Symposium on Parallel and Distributed Processing*, pages 1–12, 2010.